Hydrodynamic correlations and diffusion coefficient of star polymers in solution

Sunil P. Singh, Chien-Cheng Huang, Elmar Westphal, Gerhard Gompper, and Roland G. Winkler

Citation: The Journal of Chemical Physics **141**, 084901 (2014); doi: 10.1063/1.4893766
View online: http://dx.doi.org/10.1063/1.4893766
View Table of Contents: http://scitation.aip.org/content/aip/journal/jcp/141/8?ver=pdfcov
Published by the AIP Publishing

Hydrodynamic correlations and diffusion coefficient of star polymers in solution

Sunil P. Singh,[1,2,a)] Chien-Cheng Huang,[1] Elmar Westphal,[3] Gerhard Gompper,[1,b)] and Roland G. Winkler[1,c)]

[1]*Institute of Complex Systems and Institute for Advanced Simulation, Forschungszentrum Jülich, D-52425 Jülich, Germany*
[2]*Department of Polymer Science and Engineering, University of Massachusetts, Amherst, Massachusetts 01003, USA*
[3]*Peter Grünberg Institute and Jülich Centre for Neutron Science, Forschungszentrum Jülich, D-52425 Jülich, Germany*

(Received 18 June 2014; accepted 12 August 2014; published online 26 August 2014)

The center-of-mass dynamics of star polymers in dilute solution is analyzed by hybrid mesoscale simulations. The fluid is modeled by the multiparticle collision dynamics approach, a particle-based hydrodynamic simulation technique, which is combined with molecular dynamics simulations for the polymers. Star polymers of various functionalities are considered. We determine the center-of-mass velocity correlation functions, the corresponding mean square displacements, and diffusion coefficients. The velocity correlation functions exhibit a functionality-dependent and structure-specific intermediate time regime, with a slow decay. It is followed by the long-time tail $t^{-3/2}$, which is solely determined by the fluid. Infinite-system-size diffusion coefficients are determined from the velocity correlation function by a combination of simulation and analytical results, as well as from the center-of-mass mean square displacement for various systems sizes and extrapolation. In terms of the hydrodynamic radius, the star polymer hydrodynamic diffusion coefficient exhibits the same universal system-size dependence as a spherical colloid. The functionality dependence of the ratio of hydrodynamic radii and the radii of gyration agrees well with experimental predictions. © *2014 AIP Publishing LLC*. [http://dx.doi.org/10.1063/1.4893766]

I. INTRODUCTION

The fundamental relevance of fluid-mediated interactions for the dynamics of polymers dissolved in a fluid is well established.[1–5] Experiments on synthetic[6–10] and biological flexible and semiflexible polymers,[11–20] analytical theory,[1–5,19,21–31] and computer simulations[32–46] corroborate the presence and significance of hydrodynamic interactions. Moreover, recent combined experimental, theoretical, and simulation studies of a trapped colloidal particle in solution reveal the effect of hydrodynamic fluctuations and correlations on the colloid dynamics.[47] Fluid "memory" leads to colored, non-white, thermal fluctuating forces,[47] i.e., hydrodynamic self-interactions lead to a self-awareness of the colloidal particle.[48]

Typically, linear polymers and their long-time and large-scale dynamics are considered. In comparison, little attention has been paid to their short-time behavior, where fluid fluctuations are important.[46,47,49,50] Moreover, the impact of hydrodynamic fluctuations on the dynamics of more complex polymer architectures such as star polymers has not been addressed at all.

To gain insight into the fluid-mediated interactions in star polymers, we perform mesoscale hydrodynamic simulations by combining the multiparticle collision dynamics (MPC) approach[51] for the fluid with molecular dynamics simulations (MD) for polymers.[52,53] MPC is a particle-based simulation technique which incorporates thermal fluctuations, provides hydrodynamic correlations, and is easily coupled with other simulation techniques such as molecular dynamics simulations for embedded particles.[46,51–53] It has successfully been applied to study equilibrium and non-equilibrium dynamical properties of linear[41,43,46,52–57] and star polymers.[58–62]

In this article, we present results of the center-of-mass dynamics of star polymers for various arm numbers (functionalities). We determine the center-of-mass velocity autocorrelation function (VACF), which reflects fluid fluctuations. The correlation function exhibits a star-polymer-specific time regime for short times, which depends on the arm number, and crosses over to a universal, fluid-determined long-time tail with the power-law dependence $t^{-3/2}$, as observed for linear polymers.[46,49,50] The simulation results are well described by an analytical expression derived from the Landau-Lifshitz Navier-Stokes fluctuating hydrodynamic equations[46] for small arm numbers. For larger functionalities, additional effects lead to a faster decay of the correlation function in the polymer-specific time range. Exploiting the asymptotic behavior of the analytical solution, we determine the infinite-system-size diffusion coefficient, at least for small functionalities. In addition, the center-of-mass mean square displacement is analyzed. Simulations for various system sizes are performed to obtain the asymptotic diffusion coefficient and the hydrodynamic radius. The diffusion

a)sunilsps@gmail.com
b)g.gompper@fz-juelich.de
c)r.winkler@fz-juelich.de

coefficient decreases significantly with increasing functionality. Thereby, the hydrodynamic radius increases faster with functionality than the radius of gyration, in agreement with experiments.[63]

The paper is organized as follows. In Sec. II, the MPC method is described, the star polymer model is introduced, and the implemented parameters are summarized. The theoretical background is outlined in Sec. III, and a theoretical model is presented. Section IV presents results on the velocity correlation function and diffusive dynamics of star polymers, and Sec. V summarizes our findings.

II. MODEL

A. Multiparticle collision dynamics

In the MPC method, the fluid is described by N_s point particles of mass m, with continuous values of the positions $\boldsymbol{r}_i$ and velocities $\boldsymbol{v}_i$ $(i = 1, \ldots, N_s)$. Their dynamics proceeds in two steps—the streaming and collision steps.[51–53] In the streaming step, the fluid particles move ballistically with their respective velocities, and their positions are updated according to

$$\boldsymbol{r}_i(t + h) = \boldsymbol{r}_i(t) + h\boldsymbol{v}_i(t), \tag{1}$$

where h is denoted as collision time. In the collision step, the particles are sorted into cubic cells of linear dimension a. Particles within a cell interact with each other by a stochastic process. Here, we apply the stochastic rotation dynamics approach (SRD),[51–53,64] where the relative velocities of the particles, with respect to the center-of-mass velocity of the cell, are rotated around a randomly oriented axis by an angle α. The orientation of the axis is chosen independently for every cell and in every step. The particle velocities are then given by

$$\boldsymbol{v}_i(t + h) = \boldsymbol{v}_{cm}(t) + \boldsymbol{\mathcal{R}}(\alpha)(\boldsymbol{v}_i(t) - \boldsymbol{v}_{cm}(t)), \tag{2}$$

where

$$\boldsymbol{v}_{cm} = \frac{1}{N_c}\sum_{j=1}^{N_c}\boldsymbol{v}_j \tag{3}$$

is the center-of-mass velocity of the cell of particle i, and N_c is the number of the fluid particles in the cell. $\boldsymbol{\mathcal{R}}$ denotes the rotation operator.[65] In this process mass, energy, and momentum are conserved, which ensures the buildup of correlations between particles and gives rise to hydrodynamic interactions. The partition of space in collision cells implies a violation of Galilean invariance;[64] it can be restored by performing a random shift of the collision grid at every step.[64]

B. Star polymer

A star polymer is comprised of f flexible polymer arms, each with N_m monomers of mass M, which are attached to a common center by one of their ends. For illustration, a simulation snapshot is displayed in Fig. 1. The polymers are modeled as linear bead-spring chains, where consecutive monomers are connected by a harmonic potential according to

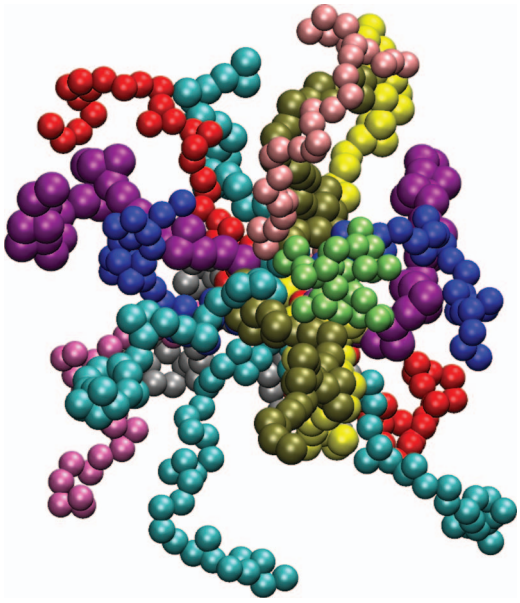

FIG. 1. Simulation snapshot of a star polymer with $f = 20$ polymer arms of $N_m = 30$ monomers each at equilibrium. For better visibility, the various arms are colored differently.

$$V_b = \frac{\kappa_b}{2}\sum_{k=1}^{N_m-1}(|\boldsymbol{R}_{k+1} - \boldsymbol{R}_k| - l)^2. \tag{4}$$

$\boldsymbol{R}_k$ denotes the position of particle k, and l is the bond length. Excluded-volume interactions between non-bonded monomers are accounted for by the shifted, truncated, and repulsive Lennard-Jones (LJ) potential

$$V_{LJ} = 4k_BT\left[\left(\frac{\sigma}{R}\right)^{12} - \left(\frac{\sigma}{R}\right)^{6} + \frac{1}{4}\right], \tag{5}$$

for monomer distances $R \le \sqrt[6]{2}\sigma$, and $V_{LJ} = 0$ otherwise. The symbol k_B denotes Boltzmann's constant, T is the temperature, and σ characterizes the diameter of a monomer. To avoid a strong monomer overlap in the star center, the bond length l_c and σ_c for the central particle are set to twice the values of the other monomers.

The dynamics of the monomers is described by Newton's equations of motion, which we solve by the velocity Verlet algorithm.[66,67]

The coupling of the fluid with a star polymer can be realized by various means. A very efficient way is to include the monomers in the collision step.[41,53,68] Hence, in cells with monomers, the center-of-mass velocity is given by

$$\boldsymbol{v}_{cm}(t) = \frac{\sum_{i=1}^{N_c} m\boldsymbol{v}_i(t) + \sum_{k=1}^{N_c^m} M\boldsymbol{V}_k(t)}{mN_c + MN_c^m}, \tag{6}$$

where N_c^m is the number of monomers within the considered cell. The velocity $\boldsymbol{V}_k$ of monomer k after a collision follows according to Eq. (2).

In order to maintain a constant temperature, a local Maxwellian thermostat—the Maxwell-Boltzmann scaling method (MBS)—is applied at every collision step and cell.[69]

C. Parameters

The transport properties of the MPC fluid are determined by the collision time h, the rotation angle α, and the mean number of fluid particles per collision cell $\langle N_c \rangle$.[52,53,57] By tuning these parameters, we attain a fluid with a high Schmidt number and a low Reynolds number Re. The choice $\langle N_c \rangle = 10$, $\alpha = 130^\circ$, and $h/\sqrt{ma^2/(k_BT)} = 0.1$, yields the fluid viscosity $\eta = 8.7\sqrt{mk_BT/a^4}$ and the Schmidt number Sc = 17, which ensures that momentum transport dominates over mass transport.[53] Note, the equation of state of the MPC fluid is that of an ideal gas, thus, the velocity of sound is $c = \sqrt{k_BT/m}$.

For a polymer, we use the parameters $M = 10m$, the bond length $l/a = 1$, and $\kappa_b = 10^3 k_BT/l^2$. The Lennard-Jones parameter σ is set to $\sigma/l = 0.8$. The time step of the velocity Verlet algorithm is $h/20$. Stars with $f = 5$, 10, 20, 40, and 50 arms are considered with $N_m = 30$ monomers. In addition, stars with short polymer arms of length $N_m = 10$ and functionality $f = 50$ are studied for comparison.

A cubic simulation box is adopted and three-dimensional periodic boundary conditions are applied. The box lengths $L/a = 30$, 50, 70, 90, 110, and 140 are considered. This corresponds to the maximum number of fluid particles $N_s = 2.7 \times 10^7$. In all cases, a single star polymer is considered to avoid effects due to inter-star-polymer interactions. At least 50 independent simulation runs of approximately 10^6 collisions are performed for every setup to arrive at a satisfactory statistical accuracy.

For an efficient simulation, we exploit a Graphics Processing Unit (GPU) version of our MPC algorithm.[65] Thereby, the fluid dynamics is treated by a GPU and the equations of motion for the star polymers are integrated on a Central Processing Unit (CPU). This yields a significant performance enhancement compared to a single CPU code. For a system of size $L/a = 140$ and 10^6 MPC steps, the total run time is on the order of two days on a single GPU.

III. THEORETICAL CONSIDERATIONS

A. Diffusion coefficient

The diffusion coefficient D of a molecule follows as integral over the center-of-mass velocity correlation function $\langle \boldsymbol{V}_{cm}(t) \cdot \boldsymbol{V}_{cm}(0) \rangle$ according to

$$D = \frac{1}{3} \int_0^\infty \langle \boldsymbol{V}_{cm}(t) \cdot \boldsymbol{V}_{cm}(0) \rangle dt, \tag{7}$$

with the center-of-mass velocity $\boldsymbol{V}_{cm}(t)$. Equivalently, in the asymptotic limit $t \to \infty$, D follows from the corresponding Einstein relation for the mean square displacement

$$\langle (\boldsymbol{R}_{cm}(t) - \boldsymbol{R}_{cm}(0))^2 \rangle = 6Dt \tag{8}$$

of the polymer center-of-mass $\boldsymbol{R}_{cm}(t)$.[66,70]

As is well known, hydrodynamic interactions are of long-range character and velocity correlations exhibit a long-time tail.[2,46,71–79] As a consequence, the diffusion coefficient depends on the systems size for periodic systems,[33,34,36,80,81] due to the suppression of long-wavelength hydrodynamic modes.[79]

For a periodic system, the finite-system-size self-diffusion coefficient D_L of a *spherical* particle of radius R_H in a periodic system can be written as

$$D_L = D - \frac{k_BT}{6\pi\eta L}\left(2.837 - \frac{4\pi R_H^2}{3L^2}\right), \tag{9}$$

up to third order in the simulation box size L^{-1}.[82,83] The asymptotic diffusion coefficient D itself is related to the hydrodynamic radius R_H via

$$D = \frac{k_BT}{6\pi\eta R_H} \tag{10}$$

for no-slip boundary conditions on the sphere surface.

At large distance, we expect the flow field around a star polymer to be similar to that around a spherical particle, as also assumed for a linear polymer in Ref. 83. Therefore, Eq. (9) should also apply to our star-polymer system.

The diffusion coefficient of a polymer structure is determined by local friction, i.e., diffusion of the monomers themselves, and intramolecular hydrodynamic interactions.[18,19,27,34,36,41,46] Hence, for a *star polymer*, we set

$$D_L = \frac{D_L^0}{fN_m + 1} + D_L^H, \tag{11}$$

where D_L^0 is the self-diffusion coefficient of a single monomer and D_L^H is determined by hydrodynamic interactions between the various monomers. Both terms are affected by periodic boundary conditions.

For a monomer of mass $M = 10m$ and the time step $h/\sqrt{ma^2/(k_BT)} = 0.1$, simulations yield the diffusion coefficient $D_0/\sqrt{k_BTa^2/m} = 0.02$, which implies the hydrodynamic radius $r_H/a = 0.3$. Since the hydrodynamic radius r_H of a monomer is much smaller than the system size, $r_H/L \leq 10^{-2}$ for all considered systems, we can neglect finite system-size corrections for the monomer diffusion. Moreover, the total number of monomers is much larger than unity, $fN_m + 1 > 150$, thus, the finite-size correction for the monomer diffusion coefficient is much smaller than that due to intramolecular hydrodynamic interactions. Therefore, we consider

$$D_L^H = D_L - \frac{D_0}{fN_m + 1} \tag{12}$$

in the following, and determine a star-polymer hydrodynamic radius according to

$$D_L^H = \frac{k_BT}{6\pi\eta R_H} - \frac{k_BT}{6\pi\eta L}\left(2.837 - \frac{4\pi R_H^2}{3L^2}\right), \tag{13}$$

from which we obtain the infinite-system-size diffusion coefficient $D^H = k_BT/(6\pi\eta R_H)$.

B. Velocity autocorrelation function

The velocity autocorrelation function of a star polymer is governed by intramolecular polymer-polymer interactions as well as the conformational properties of individual arms. To arrive at an analytical expression for the VACF, we adopt a

fluctuating hydrodynamics approach, which provides excellent agreement with MPC simulation data for polymers in dilute solution.[46] Thereby, the fluid is considered as a continuum and is described by the linearized Landau-Lifshitz Navier-Stokes equations. Under the assumption of no-slip boundary conditions, the center-of-mass velocity of the star polymer is approximated by

$$\boldsymbol{V}_{cm}(t) = \frac{1}{N_m}\sum_{i=1}^{N_m} \boldsymbol{v}^R(\boldsymbol{R}_i, t), \tag{14}$$

where $\boldsymbol{v}^R(\boldsymbol{R}_i, t)$ is the random fluid velocity due to thermal fluctuations at the position $\boldsymbol{R}_i$ of monomer i and time t. The correlation function of the random velocity within the linearized Landau-Lifshitz Navier-Stokes equations is

$$\langle \boldsymbol{V}_{cm}(t)\cdot\boldsymbol{V}_{cm}(0)\rangle = \frac{1}{N_m}\frac{k_BT}{V}\sum_{\boldsymbol{k}} S(\boldsymbol{k})[2Q^T(\boldsymbol{k},t)+Q^L(\boldsymbol{k},t)] \tag{15}$$

for a finite periodic simulation box, with the wave-vector components $k_\beta = 2\pi n_\beta/L$, $n_\beta \in \mathbb{Z}$, $\beta \in \{x, y, z\}$, and $\boldsymbol{k} \neq 0$.[46,79] S denotes the structure factor of a star polymer

$$S(\boldsymbol{k}) = \frac{1}{N_m}\sum_{i,j}\langle e^{i\boldsymbol{k}\cdot(\boldsymbol{r}_i-\boldsymbol{r}_j)}\rangle, \tag{16}$$

and the terms Q^T and Q^L are the hydrodynamic functions of the transversal and longitudinal hydrodynamic modes, which are explicitly given in the Appendix.[46,79] The structure factor (16) captures the star polymer aspects, whereas the hydrodynamic functions are solely determined by the fluid properties. This approach applies above a minimum length scale only, since the continuum solution of the Navier-Stokes equations is used, which does not apply to the MPC fluid on length scales below the cell size a.[79] Moreover, star polymer inertia effects are neglected. Hence, the theoretical approach applies above a certain time scale only.

In Ref. 46, we derived analytical expressions for the VACF of individual phantom and self-avoiding polymers. As an important result, we found a polymer-specific power-law time regime for $R_G/c \ll t \ll R_G^2/\mu$, where the velocity correlation function decays as $(R_G^2)^{-1/(2\nu)}(\mu t)^{1/(2\nu)-3/2}$. Here, R_G is the radius of gyration, c the velocity of sound, μ the kinematic viscosity of the fluid, and ν the polymer scaling exponent; $\nu = 1/2$ and $\nu \approx 3/5$ for phantom and self-avoiding polymers, respectively. R_G/c corresponds to the time for sound to traverse the size of the polymer, and R_G^2/μ is the time for hydrodynamic vorticity propagation over the same distance. For times $t \gg R_G^2/\mu$, the VACF exhibits the long-time tail $(\mu t)^{-3/2}$, which is determined by the fluid only.

IV. RESULTS

A. Center-of-mass velocity correlation function

Figure 2 displays normalized star-polymer center-of-mass velocity correlation functions,

$$C_v(t) = \frac{m}{k_BT}\langle \boldsymbol{V}_{cm}(t)\cdot\boldsymbol{V}_{cm}(0)\rangle, \tag{17}$$

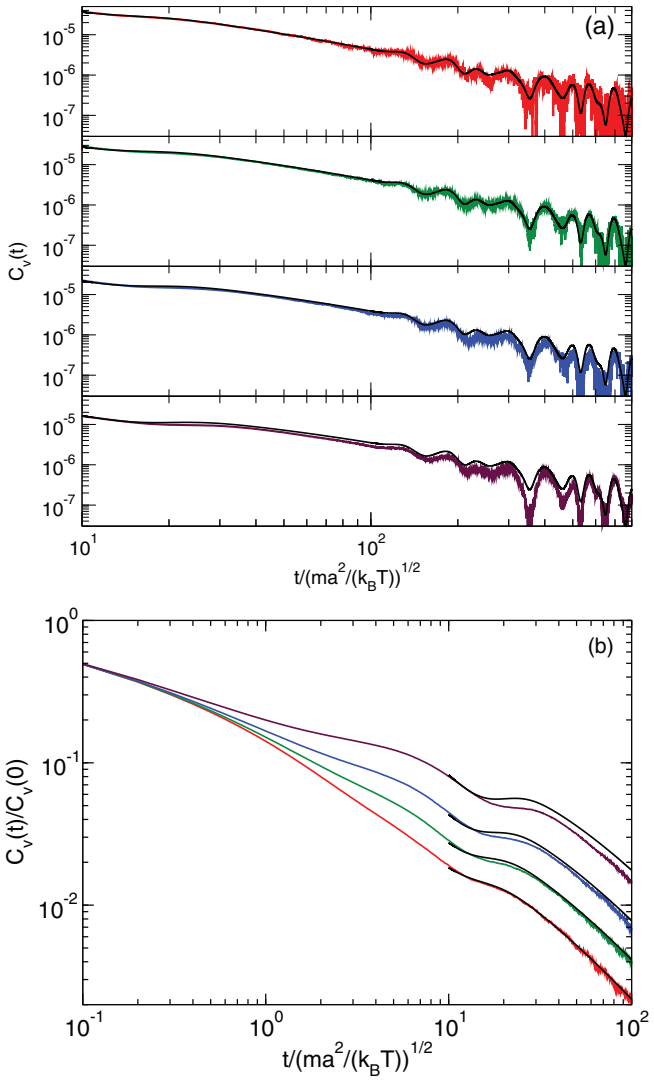

FIG. 2. Center-of-mass velocity autocorrelation functions of star polymers for the arm length $N_m = 30$ and the box size $L/a = 140$. (a) Long time behavior for the functionalities $f = 5, 10, 20$, and 50 (top to bottom). (b) Short time behavior with $f = 5, 10, 20$, and 50 (bottom to top). The black lines are calculated using the theoretical expression (15).

for various functionalities. We observe a clear dependence on functionality, where the correlation function decreases in magnitude with increasing f. In agreement with the equipartition theorem, we find $C_v(0) = 3/[10(fN_m + 1)]$. As shown in Fig. 2(b) for $C_v(t)/C_v(0)$, the correlation functions for the various functionalities decay in the same way during the first collision step.[41] This decay is determined by the average number of monomers in a collision cell, which is equal for all considered f. Only afterwards hydrodynamic correlations build up, which leads to a splitting of the correlation functions with stronger correlations for the higher functional star polymers.

The minimum at $t \approx 10\sqrt{ma^2/(k_BT)}$ reflects backtracking effects due to sound propagation of the compressible MPC fluid.[78,84] Thereby, the effect becomes more pronounced with increasing arm number. Moreover, sound is responsible for the oscillations of the correlation functions for $t \gtrsim L/c$ (Fig. 2(a)). The periodic boundary conditions imply a reoccurrence of fluid sound waves after traversing the simulation box. Figure 3 illustrates the system-size dependence of the

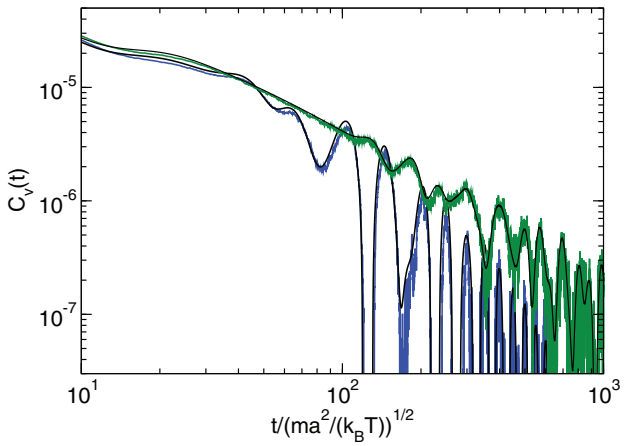

FIG. 3. Center-of-mass velocity autocorrelation functions of a star polymer with $f = 10$ arms of length $N_m = 30$ for the system sizes $L/a = 50$ (bottom) and $L/a = 140$ (top). The solid lines (black) are calculated using the theoretical expression (15).

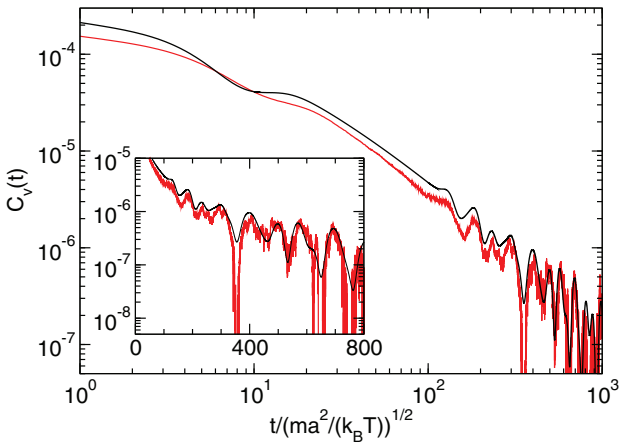

FIG. 4. Normalized center-of-mass velocity autocorrelation function of a star polymer with functionality $f = 50$ and arm length $N_m = 10$ in a simulation box of size $L/a = 140$ (red). The black line is calculated using the theoretical expression (15). The inset shows the same function on a linear scale.

correlation function. For $L/a = 50$, the oscillations set in at earlier times than for $L/a = 140$, the variations are more pronounced, and C_v assumes negative values. Moreover, the correlation function for $L/a = 50$ shows the exponential decay in the asymptotic limit of long times.[79] Evidently, the finite system size affects the correlation function even at rather short times. Only for systems larger than $L/a \approx 100$, we find a system-size independent correlation for $t/\sqrt{ma^2/(k_BT)} \lesssim 80$. This suggests that a minimum system size is required to achieve an accurate correlation function and ultimately a suitable diffusion coefficient.

The results of the analytical expression (15), with the respective star-polymer structure factors of Ref. 61, are also shown in Figs. 2 and 3. The theoretical approach matches the simulated correlation function for $f = 5$ very well. However, with increasing functionality the agreement becomes worse; for $f = 50$ there is a considerable mismatch between simulation data and theory over almost the whole displayed time scale. The theoretical curves for the various f merge into a universal dependence for long times, which reflects the fact that in the asymptotic limit $C_v(t)$ is independent of any star-polymer property and only depends on fluid correlations (see also Fig. 6). We expect the simulation data to exhibit the same behavior, however, the limit might only be reached for times beyond those accessible in simulations with reasonable accuracy.

To shed light on the long-time behavior, we study a star polymer with $f = 50$ arms of length $N_m = 10$ only. Since its radius of gyration is smaller, we expect to reach the asymptotic limit earlier. The simulation data are compared with the theoretical expression in Fig. 4. As for the longer-arm stars, we observe a significant difference between the theoretical prediction and the simulation data over a wide time range. However, for times $t \gtrsim 400\sqrt{ma^2/(k_BT)}$, the theoretical expression reproduces the simulation results rather well. Hence, the hydrodynamic behavior of a star polymer on long-time scales is solely governed by fluid fluctuations.

Interestingly, the correlation functions for the higher-functionality stars can very well be described by the theoretical expression, when a somewhat larger viscosity is used. Such an increase in the frictional properties could be attributed to enhanced polymer-polymer interactions in dense stars, e.g., in the denser and more extended core region. However, this modified description would only apply over a certain time range, since in the asymptotic long-time limit the fluid viscosity should determine the decay of the correlation function. To account for the observed deviations, an improved theoretical description is desirable. Thereby, the dynamic structure factor rather than only the static one may have to be taken into account.

B. Center-of-mass mean square displacement

Figure 5 provides an example of the center-of-mass mean square displacement (MSD),

$$\Delta R_{cm}^2 = \langle (\boldsymbol{R}_{cm}(t) - \boldsymbol{R}_{cm}(0))^2 \rangle, \tag{18}$$

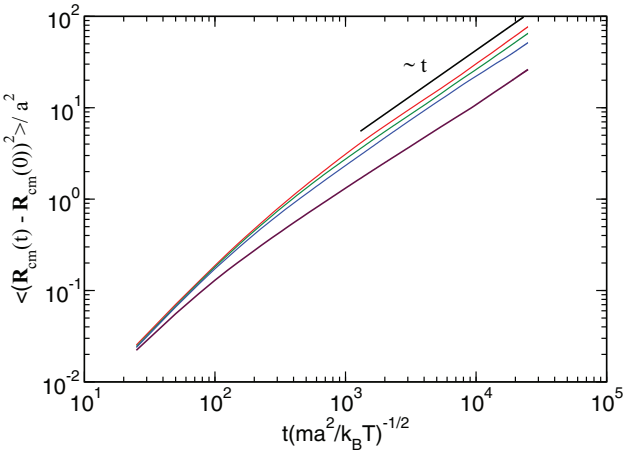

FIG. 5. Center-of-mass mean square displacements of star polymers of functionality $f = 20$ for the system sizes $L/a = 30, 50, 70, 110$ (bottom to top). The straight line indicates the linear time dependence $\langle (\boldsymbol{R}_{cm}(t) - \boldsymbol{R}_{cm}(0))^2 \rangle \sim t$.

for various system sizes. At short times, ΔR_{cm}^2 increases somewhat stronger than linearly with time due to inertia effects. For longer times, the MSD reaches the linear diffusive regime. As expected, we find a pronounced system-size dependence, with a slower dynamics in a smaller simulation box.

C. Diffusion coefficient

Here, we determine the infinite-system-size center-of-mass diffusion coefficient for stars of various functionalities. We exploit both, the velocity correlation function as well as the mean square displacement.

1. Velocity correlation function

Finite-size effects in the correlation function C_v manifest themselves as oscillations for $t \gtrsim L/c$ and an exponential damping for even longer times.[79] Thereby, the oscillations shift to longer time scales with increasing system size and vanish completely for an infinite system (cf. Fig. 3). Figure 6 presents correlation functions C_v for finite systems and the corresponding asymptotic ones in comparison with the simulation data. The theoretical correlations for an infinite system agree well with those for finite systems above $t \approx R_g/c$. Hence, we suggest the following procedure to obtain the diffusion coefficient (7). We combine the numerically obtained correlation functions below a certain time, where finite-size effects or not yet present, with the analytical infinite-system-size function above that time and integrate the combined correlation function.

The time dependence

$$D(t) = \frac{1}{3}\int_0^t \langle \boldsymbol{V}_{cm}(t') \cdot \boldsymbol{V}_{cm}(0)\rangle dt' \qquad (19)$$

of integrated correlation functions is displayed in Fig. 7 . Evidently, there is a significant functionality dependence. For every functionality, three different curves are shown: the bare

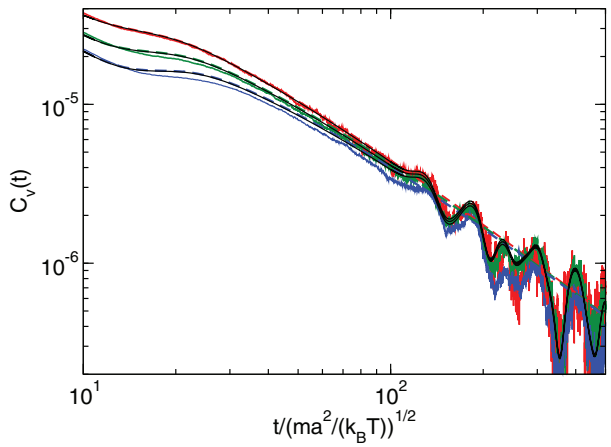

FIG. 6. Normalized center-of-mass velocity autocorrelation function of star polymers with functionalities $f = 5$, 10, and 20 (top to bottom) and arm length $N_m = 30$ in a simulation box of size $L/a = 140$. The solid black lines indicate the analytical solution (15) for the finite system and the dashed lines the solution for an infinite system.

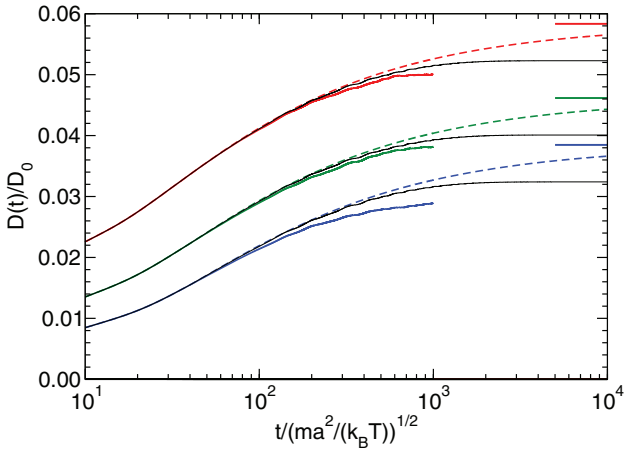

FIG. 7. Time dependence of the integral of the VACF (19) for star polymers of functionality $f = 5, 10$, and 20 (top to bottom) with $N_m = 30$ in a periodic box of length $L/a = 140$. The colored solid lines (bottom) are integrals of the bare simulation data. The dashed lines are obtained by a combination of simulation data for $t \leqslant t_c/\sqrt{ma^2/(k_BT)} = 40$ and the infinite system-size analytical correlation function, whereas for the black lines (middle) the finite system-size analytical correlation function is used. D_0 is the diffusion coefficient of an individual monomer.

finite-system-size integral, the integral of the combined set of the simulation data for $t \leqslant t_c/\sqrt{ma^2/(k_BT)} = 40$ and the finite-size analytical expression for larger times, and similarly, the simulation data combined with the infinite system size analytical expression. For the functionalities $f = 5$ and 10, the combined curves compare well with the pure simulation-based curves even considerably above the time t_c. The worse agreement of the analytical expression with the simulation data for $f = 20$ (cf. Fig. 6) is reflected in the earlier splitting of the theory-based curves from that of the bare simulation data.

The finite and infinite system-size theoretical VACFs agree well for $t > t_c$. Significant deviations between these curves appear as soon as sound undulations become important and, more importantly, the finite-size correlation functions start to decay exponentially. The latter implies the quantitative difference between the finite-system size $D(t)$ integrals, which assume a constant value at large times, and the infinite system asymptotic values, which are indicated by horizontal bars on the right. We like to emphasize that sound is not contributing to the diffusion coefficient, as is well known.[46] The diffusion coefficients themselves are listed in Table I.

TABLE I. Values for the radius of gyration R_G, hydrodynamic radius R_H, and diffusion coefficient D_H—extrapolated to infinite system size—for dilute solutions of star polymers of functionality f. D_0 is the diffusion coefficient of an individual monomer. The diffusion coefficients D_H^v (last column) are extracted from the center-of-mass velocity autocorrelation function, whereas the other ones are obtained by the center-of-mass mean square displacement.

f	R_G/l	R_H/l	R_H/R_G	D_H/D_0	D_H^v/D_0
5	6.3	6.1	0.97	0.050	0.051
10	7.1	7.5	1.05	0.041	0.042
20	7.9	9.2	1.16	0.033	0.035
40	8.9	11.3	1.27	0.027	...
50	9.2	12.0	1.30	0.026	...

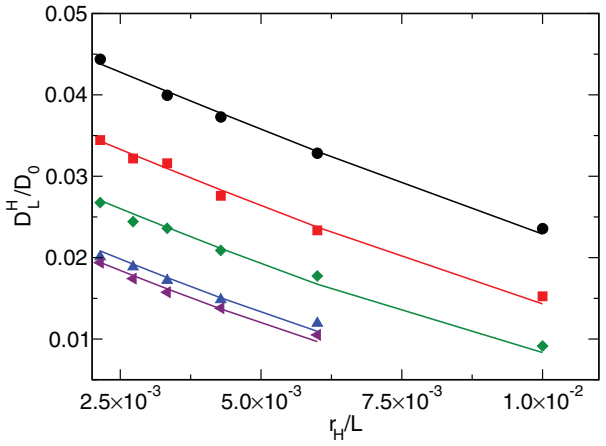

FIG. 8. Hydrodynamic part of the diffusion coefficients of star polymers as a function of system size L for the functionalities $f = 5$, 10, 20, 40, 50 (top to bottom). The data are obtained from the stars' center-of-mass mean square displacements. The solid lines are fits of Eq. (13) with respect to R_H. D_0 is the diffusion coefficient of an individual monomer.

2. Mean square displacement

The self-diffusion coefficient D_L of a star polymer for a finite system can be obtained from its center-of-mass mean square displacement (8) (cf. Fig. 5). Corresponding values D_L^H are presented in Fig. 8 for various systems size. As for the integrals (19), the diffusion coefficients D_L^H exhibit a strong functionality dependence—they increase with increasing system size, and approach a limiting value in the asymptotic limit $L \to \infty$. The diffusion coefficients are well described by the expression (13) within the accuracy of the simulations for all functionalities. The asymptotic values D^H and the corresponding hydrodynamic radii are summarized in Table I. Evidently, these diffusion coefficients agree very well with those obtained from the velocity correlation functions.

Figure 9 displays the scaled diffusion coefficients D_L^H/D_H as function of the R_H/L, i.e., the value $D^0/(fN_m + 1)$ has been subtracted from the diffusion coefficient extracted from the mean square displacement. The obtained data follow the predicted dependence well. Evidently, higher order corrections $\mathcal{O}((R_H/L)^3)$ cannot be neglected for the considered range of R_H/L values. Interestingly, our star polymers exhibit the same system-size dependence as spherical colloids[82,85–87] and linear polymers.[34,83] At a first glance, this seems to be obvious, because the first-order correction term is independent of the star-polymer size. For our system sizes, however, higher order corrections are required to adequately describe the simulation results, where we characterize the size of a star polymer by the hydrodynamic radius. Hence, the hydrodynamic radius seems to be a suitable quantity to characterize the size of the star polymer in diffusion.

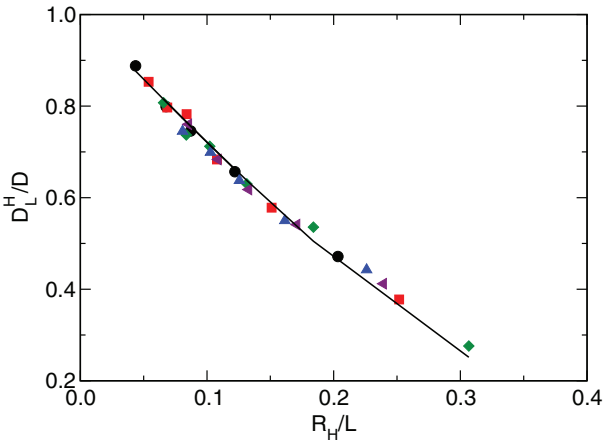

FIG. 9. Scaled diffusion coefficients of star polymers as function of R_H/L for the functionalities $f = 5$ (bullets), 10 (squares), 20 (diamonds), 40 (up triangle), and 50 (left triangle). The solid line corresponds to Eq. (13).

The dependence on functionality of the radius of gyration, as documented in Table I, is consistent with theoretical predictions $R_G \sim f^{(1-\nu)/2}$.[88–90] From the static structure factor of individual arms,[61] we find $\nu \approx 0.63$, a value somewhat larger than the theoretical value $\nu \approx 0.6$.[2] The difference is related to the shortness of the polymers and strong excluded-volume interactions. The values of Table I yield $R_G \sim f^{0.16}$, which is close to the theoretical expectation $R_G \sim f^{0.18}$ with $\nu = 0.63$.

Diffusion coefficients of star polymers in good solvent have been measured experimentally, and R_H values have been extracted by using the Stokes-Einstein relation for the functionality range $f = 18$–64.[63] The corresponding ratios of the hydrodynamic radii and the radii of gyration R_H/R_G are in the range 1.18–1.4.[63] These values are close to the values obtained from our simulations. In particular, we find the same qualitative dependence on f, but the experimental values are slightly larger at the same functionality. This deviation could be related to differences in arm lengths, in (micro)structural details of the cores, effective monomer sizes, or even experimental uncertainties.

V. SUMMARY AND CONCLUSIONS

We have analyzed the influence of hydrodynamic interactions on the center-of-mass dynamics of star polymers of various functionalities. Both, the velocity autocorrelation function and the mean square displacement of the star center-of-mass have been investigated.

The velocity correlation function exhibits a time regime, which is determined by the dynamics of the polymer arms. Its range strongly depends on the arm length and should show the power-law decay $t^{-2/3}$ under good-solvent conditions for arm lengths much longer than those considered here.[46] The simulations yield exponents on the order of unity. Hence, the decay is (much) slower than that of the fluid long-time tail. Moreover, the decay of the correlation function in that regime strongly depends on functionality. Thereby, the disagreement of the simulated correlation function with the theoretical prediction for $f \gtrsim 20$ suggests that inter-arm interactions play a significant role in dense stars.

Both, the velocity autocorrelation function and the mean square displacement exhibit a strong dependence on the system size due to suppression of long-wavelength hydrodynamic modes by periodic boundary conditions.[33,36,79,80] In order to extract infinite-system-size diffusion coefficients and hydrodynamic radii, we applied two approaches. On the one

hand, we used a combination of simulation and analytical results to calculate the diffusion coefficient from the velocity autocorrelation function. On the other hand, we performed a series of simulations for various system sizes, and extrapolated the corrected diffusion coefficient extracted from the star-polymer mean square displacement to infinite system sizes. The respective values agree very well with each other. Moreover, we find the same system-size dependence as for spherical colloids, when we replace the colloid radius by the hydrodynamic radius of a star polymer. In addition, the ratios of the hydrodynamic radii and the radii of gyration obtained from simulations show the same functionality dependence as experimental results.[63]

Our simulations confirm that MPC is a valuable simulation approach for the investigation of the dynamics of complex soft matter systems. Specifically, the implementation of the approach on a GPU opens a route to investigate a broad range of yet unexplored systems, in particular, systems with longer arms and higher functionalities. Without GPU usage, the study would have required considerably more computation time on CPU-based clusters, or would have been much more costly on massively parallel computers.

ACKNOWLEDGMENTS

We gratefully acknowledge financial support by the Deutsche Forschungsgemeinschaft (DFG) through the Collaborative Research Center "Physics of Colloidal Dispersions in External Fields" (SFB TR6), and by the EU through the Collaborative Research Project "NanoDirect" (NMP4-SL-2008-213948) as well as the FP7-Infrastructure project ESMI (Grant No. 262348).

APPENDIX: HYDRODYNAMIC TENSOR

The solution for the fluid velocity field $\boldsymbol{v}(\boldsymbol{k}, t)$ in Fourier space of the linearized Landau-Lifshitz Navier-Stokes is given by

$$\boldsymbol{v}(\boldsymbol{k}, t) = \int \mathbf{Q}(\boldsymbol{k}, t - t')\boldsymbol{f}(t')dt', \tag{A1}$$

with the hydrodynamic tensor $\mathbf{Q}(\boldsymbol{k}, t - t')$ and the volume force density $\boldsymbol{f}(t)$.[46,79] The tensor itself is composed of a transverse $\mathbf{Q}^T$ and longitudinal $\mathbf{Q}^L$ part, where $\mathbf{Q}(\boldsymbol{k}, t) = \mathbf{Q}^T(\boldsymbol{k}, t) + \mathbf{Q}^L(\boldsymbol{k}, t) = Q^T(\boldsymbol{k}, t)(\mathbf{E} - \mathbf{P}) + Q^L(\boldsymbol{k}, t)\mathbf{P}$. $\mathbf{P}$ is the projection operator with the components $P_{\beta\beta'} = k_\beta k_{\beta'}/\boldsymbol{k}^2$ and $\mathbf{E}$ is the unit tensor. Explicitly, the transverse part Q^T is given by

$$Q^T(\boldsymbol{k}, t) = \frac{1}{\rho} e^{-\mu k^2 t}\Theta(t), \tag{A2}$$

where $\Theta(t)$ is Heaviside's function, $\mu = \eta/\rho$ denotes the kinematic viscosity, and ρ the mass density. For the MPC fluid, the viscosity $\eta = \eta^k + \eta^c$ is composed of a kinetic (η^k) and collisional (η^c) contribution.[91] The longitudinal part Q^L reads as

$$Q^L(\boldsymbol{k}, t) = \frac{1}{\rho} e^{-k^2\tilde{\mu}t/2} \times \left[\cos(\Omega t) - \sqrt{\frac{k^2\tilde{\mu}^2}{4c^2 - k^2\tilde{\mu}^2}}\sin(\Omega t)\right]\Theta(t) \tag{A3}$$

for $4c^2/(k^2\tilde{\mu}^2) > 1$, where $\Omega = k^2\tilde{\mu}\sqrt{4c^2/(k^2\tilde{\mu}^2) - 1}/2$ and $\tilde{\mu} = \tilde{\eta}/\rho = (\eta + \eta^k/3)/\rho$, and

$$Q^L(\boldsymbol{k}, t) = \frac{1}{\rho} e^{-k^2\tilde{\mu}t/2} \times \left[\cosh(\Lambda t) - \sqrt{\frac{k^2\tilde{\mu}^2}{k^2\tilde{\mu}^2 - 4c^2}}\sinh(\Lambda t)\right]\Theta(t) \tag{A4}$$

for $4c^2/(k^2\tilde{\mu}^2) < 1$, where $\Lambda = k^2\tilde{\mu}\sqrt{1 - 4c^2/(k^2\tilde{\mu}^2)}/2$.[79]

[1] H. Yamakawa, *Modern Theory of Polymer Solutions* (Harper & Row, New York, 1971).
[2] M. Doi and S. F. Edwards, *The Theory of Polymer Dynamics* (Clarendon Press, Oxford, 1986).
[3] R. B. Bird, C. F. Curtiss, R. C. Armstrong, and O. Hassager, *Dynamics of Polymer Liquids* (John Wiley & Sons, New York, 1987), Vol. 2.
[4] J. des Cloizeaux and G. Jannink, *Polymers in Solution: Their Modelling and Structure* (Clarendon Press, Oxford, 1990).
[5] H. C. Öttinger, *Stochastic Processes in Polymeric Fluids* (Springer, Berlin, 1996).
[6] T. A. King, A. Knox, W. I. Lee, and J. D. G. McAdam, Polymer **14**, 151 (1973).
[7] M. Adam and M. Delsanti, Macromolecules **10**, 1229 (1977).
[8] T. Nose and B. Chu, Macromolecules **12**, 590 (1979).
[9] C. C. Han and A. Z. Akcasu, Macromolecules **14**, 1080 (1981).
[10] K. Grass, U. Böhme, U. Scheler, H. Cottet, and C. Holm, Phys. Rev. Lett. **100**, 096104 (2008).
[11] S. S. Sorlie and R. Pecora, Macromolecules **23**, 487 (1990).
[12] W. Eimer and R. Pecora, J. Chem. Phys. **94**, 2324 (1991).
[13] D. E. Smith, T. T. Perkins, and S. Chu, Macromolecules **29**, 1372 (1996).
[14] R. Götter, K. Kroy, E. Frey, M. Bärmann, and E. Sackmann, Macromolecules **29**, 30 (1996).
[15] E. Stellwagen, Y. Lu, and N. C. Stellwagen, Biochemistry **42**, 11745 (2003).
[16] C. M. Schroeder, E. S. G. Shaqfeh, and S. Chu, Macromolecules **37**, 9242 (2004).
[17] C. M. Schroeder, R. E. Teixeira, E. S. G. Shaqfeh, and S. Chu, Phys. Rev. Lett. **95**, 018301 (2005).
[18] E. P. Petrov, T. Ohrt, R. G. Winkler, and P. Schwille, Phys. Rev. Lett. **97**, 258101 (2006).
[19] R. G. Winkler, S. Keller, and J. O. Rädler, Phys. Rev. E **73**, 041919 (2006).
[20] A. Bernheim-Groswasser, R. Shusterman, and O. Krichevsky, J. Chem. Phys. **125**, 084903 (2006).
[21] J. G. Kirkwood and J. Riseman, J. Chem. Phys. **16**, 565 (1948).
[22] B. H. Zimm, J. Chem. Phys. **24**, 269 (1956).
[23] M. Bixon, Annu. Rev. Phys. Chem. **27**, 65 (1976).
[24] S. F. Edwards and M. Muthukumar, Macromolecules **17**, 586 (1984).
[25] M. Fixman, Macromolecules **14**, 1710 (1981).
[26] S. R. Aragón and R. Pecora, Macromolecules **18**, 1868 (1985).
[27] L. Harnau, R. G. Winkler, and P. Reineker, J. Chem. Phys. **104**, 6355 (1996).
[28] K. Kroy and E. Frey, Phys. Rev. E **55**, 3092 (1997).
[29] R. G. Winkler, Phys. Rev. Lett. **97**, 128301 (2006).
[30] R. G. Winkler, J. Chem. Phys. **127**, 054904 (2007).
[31] R. G. Winkler, J. Chem. Phys. **133**, 164905 (2010).
[32] J. Garcia de la Torre, A. Jimenez, and J. J. Freire, Macromolecules **15**, 148 (1982).
[33] C. Pierleoni and J.-P. Ryckaert, J. Chem. Phys. **96**, 8539 (1992).

[34]B. Dünweg and K. Kremer, J. Chem. Phys. **99**, 6983 (1993).
[35]C. Aust, M. Kröger, and S. Hess, Macromolecules **32**, 5660 (1999).
[36]P. Ahlrichs and B. Dünweg, J. Chem. Phys. **111**, 8225 (1999).
[37]N. A. Spenley, Europhys. Lett. **49**, 534 (2000).
[38]P. Ahlrichs, R. Everaers, and B. Dünweg, Phys. Rev. E **64**, 040501 (2001).
[39]C. P. Lowe, A. F. Bakker, and M. W. Dreischor, Europhys. Lett. **67**, 397 (2004).
[40]R. G. Winkler, K. Mussawisade, M. Ripoll, and G. Gompper, J. Phys.: Condens. Matter **16**, S3941 (2004).
[41]K. Mussawisade, M. Ripoll, R. G. Winkler, and G. Gompper, J. Chem. Phys. **123**, 144905 (2005).
[42]W. Jiang, J. Huang, Y. Wang, and M. Laradji, J. Chem. Phys. **126**, 044901 (2007).
[43]S. Frank and R. G. Winkler, Europhys. Lett. **83**, 38004 (2008).
[44]M. Hinczewski, X. Schlagberger, M. Rubinstein, O. Krichevsky, and R. R. Netz, Macromolecules **42**, 860 (2009).
[45]C.-C. Huang, G. Sutmann, G. Gompper, and R. G. Winkler, Europhys. Lett. **93**, 54004 (2011).
[46]C.-C. Huang, G. Gompper, and R. G. Winkler, J. Chem. Phys. **138**, 144902 (2013).
[47]T. Franosch, M. Grimm, M. Belushkin, F. M. Mor, G. Foffi, L. Forró, and S. Jeney, Nature **478**, 85 (2011).
[48]U. F. Keyser, Nature **478**, 45 (2011).
[49]J. Bonet Avalos, J. M. Rubí, and D. Bedeaux, Macromolecules **24**, 5997 (1991).
[50]V. Lisy, J. Tothova, and A. V. Zatovsky, J. Stat. Mech. P01024 (2008).
[51]A. Malevanets and R. Kapral, J. Chem. Phys. **110**, 8605 (1999).
[52]R. Kapral, Adv. Chem. Phys. **140**, 89 (2008).
[53]G. Gompper, T. Ihle, D. M. Kroll, and R. G. Winkler, Adv. Polym. Sci. **221**, 1 (2009).
[54]J. F. Ryder and J. M. Yeomans, J. Chem. Phys. **125**, 194906 (2006).
[55]R. Chelakkot, R. G. Winkler, and G. Gompper, Phys. Rev. Lett. **109**, 178101 (2012).
[56]A. Nikoubashman and C. N. Likos, J. Chem. Phys. **133**, 074901 (2010).
[57]C.-C. Huang, R. G. Winkler, G. Sutmann, and G. Gompper, Macromolecules **43**, 10107 (2010).
[58]M. Ripoll, R. G. Winkler, and G. Gompper, Phys. Rev. Lett. **96**, 188302 (2006).
[59]S. P. Singh, R. G. Winkler, and G. Gompper, Phys. Rev. Lett. **107**, 158301 (2011).
[60]D. A. Fedosov, S. P. Singh, A. Chatterji, R. G. Winkler, and G. Gompper, Soft Matter **8**, 4109 (2012).
[61]S. P. Singh, D. A. Fedosov, A. Chatterji, R. G. Winkler, and G. Gompper, J. Phys.: Condens. Matter **24**, 464103 (2012).
[62]S. P. Singh, A. Chatterji, G. Gompper, and R. G. Winkler, Macromolecules **46**, 8026 (2013).
[63]D. Vlassopoulos, G. Fytas, T. Pakula, and J. Roovers, J. Phys.: Condens. Matter **13**, R855 (2001).
[64]T. Ihle and D. M. Kroll, Phys. Rev. E **63**, 020201(R) (2001).
[65]E. Westphal, S. P. Singh, C.-C. Huang, G. Gompper, and R. G. Winkler, Comput. Phys. Commun. **185**, 495 (2014).
[66]M. P. Allen and D. J. Tildesley, *Computer Simulation of Liquids* (Clarendon Press, Oxford, 1987).
[67]W. C. Swope, H. C. Andersen, P. H. Berens, and K. R. Wilson, J. Chem. Phys. **76**, 637 (1982).
[68]A. Malevanets and J. M. Yeomans, Europhys. Lett. **52**, 231 (2000).
[69]C.-C. Huang, A. Chatterji, G. Sutmann, G. Gompper, and R. G. Winkler, J. Comput. Phys. **229**, 168 (2010).
[70]J.-P. Hansen and I. R. McDonald, *Theory of Simple Liquids* (Academic Press, London, 1986).
[71]J. K. G. Dhont, *An Introduction to Dynamics of Colloids* (Elsevier, Amsterdam, 1996).
[72]B. J. Alder and T. E. Wainwright, Phys. Rev. A **1**, 18 (1970).
[73]R. Zwanzig and M. Bixon, Phys. Rev. A **2**, 2005 (1970).
[74]M. H. Ernst, E. H. Hauge, and J. M. J. van Leeuwen, Phys. Rev. A **4**, 2055 (1971).
[75]E. H. Hauge and A. Martin-Löf, J. Stat. Phys. **7**, 259 (1973).
[76]E. J. Hinch, J. Fluid Mech. **72**, 499 (1975).
[77]G. L. Paul and P. N. Pusey, J. Phys. A **14**, 3301 (1981).
[78]B. U. Felderhof, J. Chem. Phys. **123**, 044902 (2005).
[79]C.-C. Huang, G. Gompper, and R. G. Winkler, Phys. Rev. E **86**, 056711 (2012).
[80]A. A. Zick and G. M. Homsy, J. Fluid Mech. **115**, 13 (1982).
[81]J. T. Padding and A. A. Louis, Phys. Rev. E **74**, 031402 (2006).
[82]I. Yeh and G. Hummer, J. Phys. Chem. B **108**, 15873 (2004).
[83]A. J. C. Ladd, R. Kekre, and J. E. Butler, Phys. Rev. E **80**, 036704 (2009).
[84]M. Belushkin, R. G. Winkler, and G. Foffi, J. Phys. Chem. B **115**, 14263 (2011).
[85]H. Hashimoto, J. Fluid Mech. **5**, 317 (1959).
[86]B. R. A. Nijboer and T. W. Ruijgrok, J. Stat. Phys. **53**, 361 (1988).
[87]S. Poblete, A. Wysocki, G. Gompper, and R. G. Winkler, "Hydrodynamics of discrete-particle models of spherical colloids: A multiparticle collision dynamics simulation study," Phys. Rev. E (submitted).
[88]M. Daoud and J. P. Cotton, J. Phys. France **43**, 531 (1982).
[89]G. S. Grest, K. Kremer, and T. A. Witten, Macromolecules **20**, 1376 (1987).
[90]C. N. Likos, Phys. Rep. **348**, 267 (2001).
[91]R. G. Winkler and C.-C. Huang, J. Chem. Phys. **130**, 074907 (2009).